RSC Advances

PAPER

View Article Online
View Journal | View Issue

Cite this: *RSC Adv.*, 2016, **6**, 12398

Characterization of graphene edge functionalization by grating enhanced Raman spectroscopy

Yu-Ju Hung,*[a] Mario Hofmann,[b] Yang-Chin Cheng,[a] Chia-Wei Huang,[a] Kai-Wen Chang[b] and Jih-Yin Lee[a]

Received 18th October 2015
Accepted 11th January 2016

DOI: 10.1039/c5ra21717b

www.rsc.org/advances

The edges of graphene, a two-dimensional carbon allotrope, are an emerging research area with wide applications in catalysis and electronics. To improve the metrology of functionalized graphene edges we propose localized surface plasmon polariton (LSPP)-enhanced Raman spectroscopy on a metallic grating substrate. We demonstrate a large enhancement of edge related Raman features at 1450 cm^{-1} and 1530 cm^{-1} which are associated with armchair and zigzag hydrogen-terminated graphene edges, respectively. The graphene edges act as good scatterers to excite LSPP on a noble metal surface while the periodic structures boost the total Raman peaks of the graphene layer. Specifically, the scattering enhancement on the graphene edges make the edge modes strong. Our results highlight the potential of LSPP-enhanced Raman spectroscopy as an efficient characterization tool for graphene edge functionalization.

Introduction

Graphene is an ideal two-dimensional structure for study that has attracted significant attention.[1] Only recently, has the experimental study of graphene edges gained attention due to the promise of novel magnetic, electronic, and catalytic properties.[2–12] One major obstacle in conducting experimental studies on the quality and functionalization of graphene edges is their characterization. While transmission electron microscopy (TEM) and scanning tunneling microscopy (STM) can resolve the edge atom arrangement, they cannot provide scalable metrology of edge quality and chemical functionalization.[13,14] Furthermore, electron spectroscopy, which is a common technique for surface science, is not able to distinguish surface and edge functionalization and exhibits limited sensitivity to several potentially important elements such as hydrogen or lithium.[15–18]

We here propose localized surface plasmon polariton enhanced Raman spectroscopy (LSPP-Raman) on the grating scheme as a characterization technique with high selectivity to graphene edges. In LSPP, resonance between incident light and confined surface plasmons occurs at certain wavelengths which causes large enhancement of the surface electric fields. The coupling of those electric fields with a target and its phonons results in an enormously enhanced LSPP-Raman signal.[19] The grating confined plasmonic pool is especially sensitive to the graphene edges where the pumping light is efficiently enhanced and the Raman signals at the spots are scattered around.

Our experimental results show that the formation of LSPP on a grating substrate selectively enhance the intensity of two Raman features at 1450 cm^{-1} and 1530 cm^{-1} which are associated with armchair and zigzag graphene edges. Correlation of experimental and theoretical results reveal a resonance effect of the incident electric field with the grating period as the underlying mechanism of this enhancement. The presented results suggest the use of graphene-on-grating as a test bed for the study of edge functionalization and graphene metrology.

Experimental

To produce gratings, one layer of polymethylmethacrylate (PMMA) (Microchem A4) was spin-coated onto ITO glass and patterned by E-beam lithography. After the PMMA layer was developed, a 65 nm thick Au layer was sputtered on top and the sample was immersed in acetone solution for lift-off.

Graphene was grown on Cu foil under low pressure using methane following previous reports.[20] Briefly, the Cu foil substrate was pretreated by electrochemical polishing to ensure high smoothness, then a 30 minute annealing step in hydrogen was carried out to remove the oxide layer and increase the copper grain size. Graphene growth was conducted at 1000 °C by flowing methane with a pressure of 7 Torr for 70 minutes. After growth the graphene/copper sample was cooled to room temperature in a hydrogen atmosphere.

The produced graphene on Cu was then transferred onto the grating by wet etching the Cu-substrate using ferric chloride. To support the graphene during the process, a thin layer of PMMA

[a]*Department of Photonics, National Sun Yat-sen University, Kaohsiung, 80424, Taiwan. E-mail: yjhung@mail.nsysu.edu.tw*

[b]*Department of Material Science and Engineering, National Cheng Kung University, Tainan, 70101, Taiwan*

(Microchem A9) was spin coated on top. After positioning the graphene/PMMA structure on the target, the PMMA was removed by acetone immersion.

Raman spectroscopy was performed on a commercial micro-Raman setup (HORIBA HR800) using a 100× objective with N.A. 0.9. For each sample at least 3 spectra were taken at random positions and individually fitted.

Results and discussion

Fig. 1(a) shows the structure of the investigated samples. Due to graphene's high mechanical strength it is suspended on top of the gold grating even after removal of the PMMA supporting layer. SEM characterization reveals the presence of tears in the graphene film that are thought to originate from the transfer process (Fig. 1(b)). Raman spectra show that the grating arrangement indeed generates a large enhancement of the Raman intensity over the signal of graphene on planar Au films as expected from surface enhanced Raman spectroscopy (Fig. 1(c)). The black curve is the signals of graphene on transparent ITO glass substrate. Surprisingly two prominent peaks occur at 1450 cm^{-1} and 1530 cm^{-1} that could not be resolved on flat transparent substrate. The two peaks on the flat Au film surface is noisy and show less resonance effects.

Previous reports suggested that these two subpeaks arise from an edge-phonon coupling mode that originates from hydrogen terminated edges.[21,22] Other reports, however, found peaks in the same spectral region and associated them with residue either from PMMA[23] or adhesive tapes[24] that cannot be removed by the used solvents.

To distinguish the two possible origins of the Raman peak, we carried out a post-processing step: after initial Raman measurements, we dropped ethanol onto the sample. The high surface tension during evaporation is expected to increase the adhesion between graphene and the substrate and induce additional tears. Indeed SEM images in Fig. 2(a) reveal a higher density of edges after ethanol evaporation.

Raman spectra taken after this processing step shown in Fig. 2(b) exhibit an increase of the two features at 1450 cm^{-1} and 1530 cm^{-1} which confirms that the tearing induced edges are responsible for these peaks. Furthermore, our spectra show differences in peak width and intensity ratios compared to the observed impurities. We therefore term the observed peaks "edge-modes".

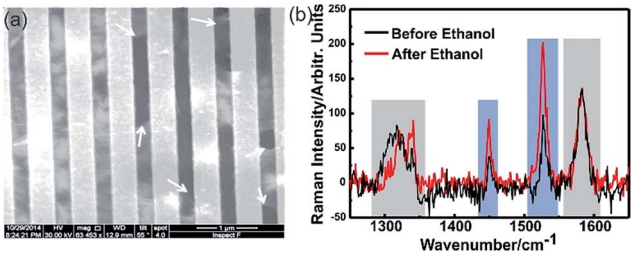

Fig. 2 (a) The SEM image of the graphene film after ethanol deposition (b) Raman spectrum of graphene layer on Au gratings before and after ethanol deposition.

We confirm this hypothesis by high-resolution mapping of the Raman features across the grating. Fig. 3(a) shows a graphene edge supported on the grating. We observe an enhanced edge-mode ratio originating from this feature (Fig. 3(b)). The broadening is caused by a convolution of the signal with the laser spot size and the asymmetry of the peak is thought to originate from an angle between the grating edge and the graphene edge. To accommodate these parameters, the edge-mode ratio was fitted to

$$I_{1530}/I_G = A\exp(-\alpha(x - x_e)^2) \times \mathrm{erfc}(\beta(x - x_g)),$$

where x_e is the position of the graphene edge, x_g is the position of the grating edge, and α,β are related to the beam size. The good agreement of our fitting suggests that the edge-mode is indeed enhanced when a graphene edge aligns with the grating edge.

The observed enhancement of the edge-modes is thought to originate from the coupling between surface plasmon polaritons generated by the Au grating structure and the graphene.[25,26] The employed gratings have previously shown efficient SPP excitation from tilted laser light incidence.[27] However, the pumping light utilization here is not as high as in ref. 27 due to the normal light incidence through the 100× objective lens with a focal spot of approximately 2 micrometers.

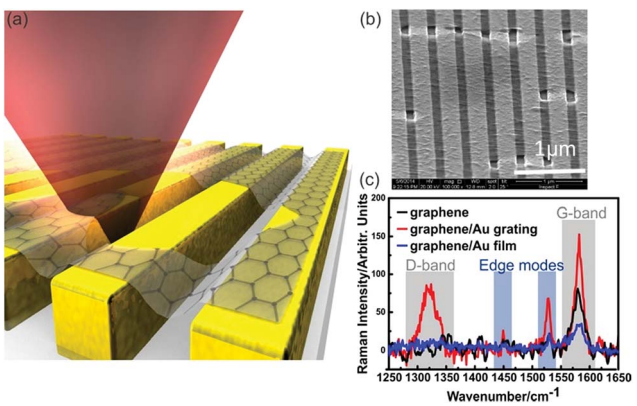

Fig. 1 (a) Sample structure, (b) SEM image of graphene on Au grating, (c) Raman spectra with and without grating structure and on glass substrate.

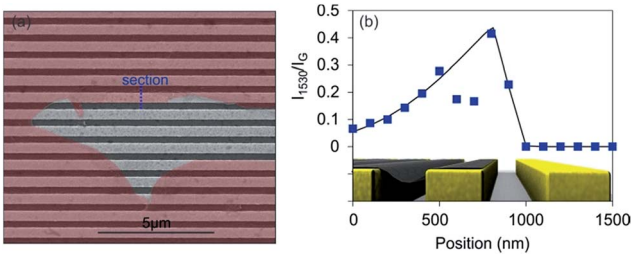

Fig. 3 (a) SEM image of investigated edge on grating, (b) normalized edge-mode intensity as a function of position, (inset) position of grating with respect to plot.

The excitation of long-range SPP requires precise control of the tilt and rotation angles to fit the momentum matching condition. Consequently, only a very limited portion of the light cone can be converted into long-range SPPs. Localized SPP (LSPP) at the graphene edges and the Au corners are expected to be dominant in the current setup. Interactions of the light with clean graphene edges are expected to be selectively enhanced due to the potential coupling of the clean and sharp graphene edges with the incident or outgoing wave vectors which greatly help the localized SPP formation. Therefore, in this paper, we have seen that the edge modes are selectively enhanced rather than G-peak.

We now investigate the effect of varying the grating period. Two contributions to the Raman signal are expected. Firstly, a larger grating period will result in a larger relative area of suspended graphene which increases the risk of tearing. Therefore, a higher edge density is anticipated. Secondly, a resonance effect between the grating period and the incident light will produce varying electric fields that enhance the Raman intensity of present graphene edges.

Fig. 4(a) shows the experimental ratios with standard deviations for graphene suspended on different grating periods. A broad maximum in Raman intensity can be seen around 600 nm which coincides with the excitation wavelength (632.8 nm). Interestingly, the intensity of the stronger 1530 cm^{-1} feature has a second peak at 744 nm that does not originate from the incident light resonance.

We simulated the localized field distribution along the graphene surface using finite element modeling (COMSOL Multiphysics) and experimental parameters with the graphene's optical constant ($n = 2.9 + 1.2i$ at 632.8 nm) from ref. 28. The top normal incidence is assumed. Fig. 4(b) shows the localized E field enhancement factor for a graphene edge that is located on a grating stripe. To be general, the locations of the graphene edge on Au grating stripe are sampled for 6 different positions and the average field strength is adopted to average out the interference effect on the grating surface. Except the grating periods, the Au stripe width also plays a proportional factor while the edge mode intensity is proportional to the Au stripe area. The simulated enhancement factor: $E_{corner}/E_{incident}$ for different Au grating periods ranges from 2–13. The field enhancement of planar Au films (65 nm thick) and SiO_2 (200 nm) on Si substrate were calculated to be 1.2 and 0.8 respectively.

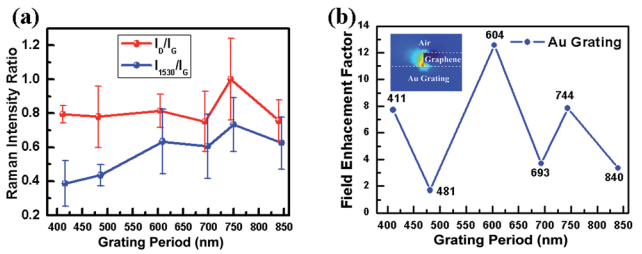

Fig. 4 (a) The peak intensity ratios with error bars: I_D and I_{1530} normalized to I_G as a function of grating period, (b) simulation of field enhancement for varying grating periods, (inset) depiction of electric field distribution.

Conclusions

In conclusion, we have demonstrated the selective enhancement of Raman graphene edge-modes through localized surface plasmon polaritons on a Au grating structure. The field enhancement is demonstrated to activate edge-phonon coupling modes which occur at 1450 cm^{-1} and 1530 cm^{-1} and are associated with hydrogen-terminated armchair and zigzag edges. The use of gratings results in a high selectivity of the edge-enhancement compared to other Raman features and enables future studies on the character and distribution of functionalized graphene edges.

Acknowledgements

We thank Prof. Chen, C.-H. from Department of Chemistry, National Sun Yat-sen University for helpful discussions on the alcohol damage case. We also thank the funding agency: Ministry of Science and Technology, Taiwan.

References

1 K. S. Novoselov, A. K. Geim, S. V. Morozov, D. Jiang, Y. Zhang, S. V. Dubonos, I. V. Grigorieva and A. A. Firsov, *Science*, 2004, **306**, 666–669.
2 L. M. Dai, *Acc. Chem. Res.*, 2013, **46**, 31–42.
3 P. Wagner, C. P. Ewels, J. J. Adjizian, L. Magaud, P. Pochet, S. Roche, A. Lopez-Bezanilla, V. V. Ivanovskaya, A. Yaya, M. Rayson, P. Briddon and B. Humbert, *J. Phys. Chem. C*, 2013, **117**, 26790–26796.
4 V. Georgakilas, M. Otyepka, A. B. Bourlinos, V. Chandra, N. Kim, K. C. Kemp, P. Hobza, R. Zboril and K. S. Kim, *Chem. Rev.*, 2012, **112**, 6156–6214.
5 H. Bai, Y. X. Xu, L. Zhao, C. Li and G. Q. Shi, *Chem. Commun.*, 2009, 1667–1669.
6 T. Kuila, S. Bose, A. K. Mishra, P. Khanra, N. H. Kim and J. H. Lee, *Prog. Mater. Sci.*, 2012, **57**, 1061–1105.
7 X. T. Jia, M. Hofmann, V. Meunier, B. G. Sumpter, J. Campos-Delgado, J. M. Romo-Herrera, H. B. Son, Y. P. Hsieh, A. Reina, J. Kong, M. Terrones and M. S. Dresselhaus, *Science*, 2009, **323**, 1701–1705.
8 X. T. Jia, J. Campos-Delgado, M. Terrones, V. Meunier and M. S. Dresselhaus, *Nanoscale*, 2011, **3**, 86–95.
9 K. Nakada, M. Fujita, G. Dresselhaus and M. S. Dresselhaus, *Phys. Rev. B: Condens. Matter Mater. Phys.*, 1996, **54**, 17954–17961.
10 Y.-W. Son, M. L. Cohen and S. G. Louie, *Phys. Rev. Lett.*, 2006, **97**, 216803.
11 C. Casiraghi, A. Hartschuh, H. Qian, S. Piscanec, C. Georgi, A. Fasoli, K. S. Novoselov, D. M. Basko and A. C. Ferrari, *Nano Lett.*, 2009, **9**, 1433–1441.
12 K. He, G.-D. Lee, A. W. Robertson, E. Yoon and J. H. Warner, *Nat. Commun.*, 2014, **5**, 3040.
13 C. O. Girit, J. C. Meyer, R. Erni, M. D. Rossell, C. Kisielowski, L. Yang, C. H. Park, M. F. Crommie, M. L. Cohen, S. G. Louie and A. Zettl, *Science*, 2009, **323**, 1705–1708.

14 J. F. Tian, H. L. Cao, W. Wu, Q. K. Yu and Y. P. Chen, *Nano Lett.*, 2011, **11**, 3663–3668.
15 K. Spyrou, D. Gournis and P. Rudolf, *ECS J. Solid State Sci. Technol.*, 2013, **2**(10), M3160–M3169.
16 B. Richard, J. Bjarke, N. Louis, A. Mie, R. Emile, B. Marco, F. Mattia, L. Erik, B. Alessandro, L. Silvano, S. Zeljko, B. Flemming, H. Bjørk, G. P. Thomas, H. Philip and H. Liv, *Nat. Mater.*, 2010, **9**, 315–319.
17 H. Kim, H.-D. Lim, S.-W. Kim, J. Hong, D.-H. Seo, D.-C. Kim, S. Jeon, S. Park and K. Kang, *Sci. Rep.*, 2013, **3**, 1506, DOI: 10.1038/srep01506.
18 Y. Cao, X. Li, I. A. Aksay, J. Lemmon, Z. Nie, Z. Yanga and J. Liu, *Phys. Chem. Chem. Phys.*, 2011, **13**, 7660–7665.
19 K. A. Willets and R. P. van Duyne, *Annu. Rev. Phys. Chem.*, 2007, **58**, 267–297.
20 Y. P. Hsieh, Y. W. Wang, C. C. Ting, H. C. Wang, K. Y. Chen and C. C. Yang, *J. Nanomater.*, 2013, 393724.
21 W. C. Ren, R. Saito, L. B. Gao, F. W. Zheng, Z. S. Wu, B. L. Liu, M. Furukawa, J. P. Zhao, Z. P. Chen and H. M. Cheng, *Phys. Rev. B: Condens. Matter Mater. Phys.*, 2010, **81**, 035412.
22 M. Kim, N. S. Safron, E. Han, M. S. Arnold and P. Gopalan, *ACS Nano*, 2012, **6**, 9846–9854.
23 Y. C. Lin, C. C. Lu, C. H. Yeh, C. H. Jin, K. Suenaga and P. W. Chiu, *Nano Lett.*, 2012, **12**, 414–419.
24 P. Klar, E. Lidorikis, A. Eckmann, I. A. Verzhbitskiy, A. C. Ferrari and C. Casiraghi, *Phys. Rev. B: Condens. Matter Mater. Phys.*, 2013, **87**, 205435.
25 W. G. Xu, X. Ling, J. Q. Xiao, M. S. Dresselhaus, J. Kong, H. X. Xu, Z. F. Liu and J. Zhang, *Proc. Natl. Acad. Sci. U. S. A.*, 2012, **109**, 9281–9286.
26 H. Raether, *Springer Tracts Mod. Phys.*, 1988, **111**, 1–133.
27 Y.-J. Hung, I. I. Smolyaninov, C. C. Davis and H.-C. Wu, *Opt. Express*, 2006, **14**, 10825–10830.
28 X. F. Wang, Y. P. Chen and D. D. Nolte, *Opt. Express*, 2008, **16**, 22105–22112.